Gallium(III) adsorption on carbonates and oxides: X-ray absorption fine structure spectroscopy study and surface complexation modeling

ARTICLE *in* JOURNAL OF COLLOID AND INTERFACE SCIENCE · NOVEMBER 2004

Impact Factor: 3.37 · DOI: 10.1016/j.jcis.2004.06.095 · Source: PubMed

3 AUTHORS, INCLUDING:

Oleg S. Pokrovsky
GET UMR 5563 CNRS, IEPS RAS Arkhangels…
243 PUBLICATIONS **4,905** CITATIONS
SEE PROFILE

Jacques Schott
French National Centre for Scientific Resea…
237 PUBLICATIONS **9,255** CITATIONS
SEE PROFILE

Available online at www.sciencedirect.com
SCIENCE DIRECT
Journal of Colloid and Interface Science 279 (2004) 314–325
JOURNAL OF Colloid and Interface Science
www.elsevier.com/locate/jcis

Gallium(III) adsorption on carbonates and oxides: X-ray absorption fine structure spectroscopy study and surface complexation modeling

O.S. Pokrovsky *, G.S. Pokrovski, J. Schott

Géochimie: Tranferts et Mécanismes, CNRS (UMR 5563)-OMP-Université Paul-Sabatier, 14, Avenue Edouard Belin, 31400 Toulouse, France

Received 5 January 2004; accepted 30 June 2004

Available online 2 September 2004

Abstract

Adsorption of Ga on calcite, magnesite, amorphous silica, and manganese oxide as a function of pH and gallium concentration in solution was studied using a batch adsorption technique. Adsorbed complexes of Ga on calcite, magnesite, and δ-MnO_2 were further characterized using XAFS spectroscopy. At high surface loadings from supersaturated solutions, Ga is likely to form a polymeric network at the surface (edge- and corner-sharing octahedra). At low surface loadings, Ga presents as isolated octahedra, probably attached to the Me–O sites on the surface, and coordinated by water molecules and hydroxide groups at 1.90–1.94 Å. At pH > 6, Ga therefore changes its coordination from 4 to 6 when adsorbing from solution ($Ga(OH)_4^-$(aq)) onto metal surface sites ($Me–O–Ga(OH)_n(H_2O)_{5-n}^{2-n}$, Me = Ca, Mg, or Mn, and $n = 1$ and 2 for carbonate minerals and MnO_2, respectively). Because the EXAFS is not capable of seeing hydrogen atoms, the protonation of surface complexes was determined by fitting the experimental pH-dependent Ga adsorption edge. A surface complexation model which assumes the constant capacitance of the electric double layer (CCM) and postulates the formation of positively charged, neutral and negatively charged surface complexes for carbonates, manganese oxide and silica, respectively, was used to describe the dependence of adsorption equilibria on aqueous solution composition in a wide range of pH and Ga concentration.

1. Introduction

It is well known that the transport and speciation of many insoluble trace elements in natural waters is essentially controlled by mineral particles and colloids [1]. Among trace elements, hydrolyzates located in the third and fourth column of the Periodic Table are the most likely to be affected by sorption processes and colloidal transport, as follows from recent ultrafiltration experiments [2–5]. In contrast to a large number of studies devoted to adsorption and colloidal behavior of divalent metals, rare earth elements, and actinides in aquatic systems [6–15], very little is known on interface equilibria of less common "insoluble" trivalent and tetravalent elements (Al, Sc, Ti, Cr, Ga, Ge, Y, Zr, In, Hf, Tl) [16–19]. Until recently, progress in studying the adsorption of these elements has been significantly hampered by analytical difficulties and poor knowledge of their aqueous speciation even at ambient temperatures. Over the past decade, important advances achieved in analytical facilities (i.e., appearance of high-resolution ICP-MS), structural characterization of metal complexes (i.e., XAFS, NMR), and conceptual understanding of solid–solution interface equilibria for multiple oxides (clays, carbonates) have allowed a more rigorous thermodynamic modeling of tri- and tetravalent element adsorption phenomena on mineral surfaces. Among trivalent elements, gallium is particularly interesting because it can be used as an analog of another more environmentally important element, aluminum [20,21], whose structures on the mineral surfaces and in aqueous solution cannot be easily accessed by XAFS spectroscopy [22]. This paper is devoted to an experimental study of Ga adsorption on four common sorbents (Ca and Mg carbonates, Mn(IV) oxide, and amorphous silica) using a combination of batch adsorption technique, XAFS spectroscopy, and surface complexation modeling.

* Corresponding author.
E-mail address: oleg@lmtg.obs-mip.fr (O.S. Pokrovsky).

0021-9797/$ – see front matter
doi:10.1016/j.jcis.2004.06.095

2. Experimental

2.1. Materials

Synthetic calcite, natural magnesite, commercial amorphous silica and synthetic δ-MnO_2 were used in the present study. Calcite was precipitated from supersaturated $(NH_4)_2CO_3 + CaCl_2$ solution at pH $\sim$ 10; magnesite crystals of natural hydrothermal origin were ground in agate pestle and mortar to produce fine powder <10-μm [23], reagent-grade Prolabo silicic acid, $SiO_2 \cdot nH_2O$, was treated in suprapure 0.1 M HNO_3 to remove the adsorbed impurities; and birnessite (δ-MnO_2) was synthesized from a $KMnO_4 + HCl$ mixture at 90 °C [24]. The crystallinity of calcite, magnesite, and birnessite was verified using X-ray diffraction. All solids were thoroughly washed in deionized Milli-Q water and conditioned in N_2-saturated, 0.01 M $NaNO_3$ or NaCl for at least one week prior the experiments. The specific BET surface areas were measured by triple-point N_2 adsorption and found to be 18.6, 0.72, 462, and 12 m^2/g for calcite, magnesite, SiO_2, and δ-MnO_2, respectively. Trace element analysis of studied solids performed by ICP-MS did not detect any impurities within $\leqslant$0.1 wt%, and Ga content was below 1 ppm. All reagents were of analytical grade or better. Suprapure $NaNO_3$ and NaCl (Merck) were used as background electrolytes.

2.2. Adsorption experiments

Adsorption experiments were carried out in acid-cleaned 30-ml polypropylene vials in a 25 ± 0.5 °C thermostated chamber. For most experiments, a mixture of $NaNO_3$ (or NaCl), HNO_3, and NaOH was used to maintain the ionic strength at 0.01 M. No buffer was used; instead, NaOH and HNO_3 were added to vary the pH. Experiments were performed by adding neutral Ga solution to preequilibrated suspension of solid. For experiments with carbonates, solutions were kept closed from the atmosphere and were buffered by the HCO_3/CO_3 ions issued from the equilibrium dissolution of the solid. Based on pH, [Ca], and [Alk] analyses of solutions, we estimated the pCO_2 in our experiments as $(2 \pm 1) \times 10^{-3}$ atm. For experiments with oxides, nitrogen-saturated $NaNO_3$ or NaCl solutions were used, prevented from contact with the atmosphere. Typical exposure time was about 1 week, although preliminary kinetic experiments performed on calcite and silica demonstrated that the full adsorption was achieved in less than 3 days. No difference in adsorbed Ga concentration on calcite was detected for exposure times of 2 weeks and 6 months. Because of high reactivity of calcite and its sensitivity to changes in solution conditions, for several samples the pH, [Ca], and [Alk] were monitored in the course of Ga adsorption experiments after 3, 7, and 14 days of exposition. No change of these parameters compared to initial equilibrium concentrations was detected within the uncertainty of analyses. At the end of experiment, pH was measured, solution was centrifuged and filtered through a 0.22-μm Nylon filter. Filtrate was acidified with ultrapure HNO_3 and kept in the refrigerator before the analysis. For experiments with carbonates, additional portion was sampled without further acidification and used for alkalinity measurements. A similar procedure was used to account for blank adsorption in our experiments. For this, supernatants obtained from mineral suspensions were conditioned in a wide range of pH at the same concentration of added Ga as in mineral adsorption experiments. After 1 week, no significant decrease of initial Ga concentration was detected upon filtration indicating on the absence of Ga adsorption on the reactor walls and Ga hydroxide formation in solutions. Only at $4 \leqslant pH \leqslant 6$ and $[Ga]_t \geqslant 10^{-4}$ M, a ~30% decrease of Ga concentration in blank experiments was observed. This was taken into account when calculating the net adsorption yield.

2.3. Analyses

For experiments with carbonates, solutions were analyzed for magnesium, calcium, alkalinity ($[Alk] = [HCO_3^-] + 2[CO_3^{2-}] + [OH^-]$), and pH. Magnesium and calcium were measured by flame atomic absorption with an uncertainty of ±1% and a detection limit of 10^{-7} and 10^{-6} M, respectively. Alkalinity was determined following a standard HCl titration procedure with an uncertainty of ±1% and a detection limit of 5×10^{-5} M. Values of pH were measured at 25 °C using a Mettler Toledo combined electrode, with an accuracy of ±0.002 units. Gallium concentration was measured by flame or flameless atomic absorption in a graphite furnace (Perkin–Elmer Zeeman 5000) over the concentration ranges 5–40 and 5–30 μg/l, respectively [20]. The reproducibility of the analysis was better than 10% and the detection limit was 3 μg/l. For Ga contents lower than 5 μg/l, analyses were performed by ICP-MS on a Perkin–Elmer Elan 6000 with a detection limit of 5 ng/l and precision of $\leqslant$5%.

2.4. Calculations

Equilibrium species distribution in solution and at the mineral surfaces were calculated for each solution composition using the MINTEQA2 code [25]. The thermodynamic constants of aqueous reactions equilibria for Ga at 25 °C were taken from Ref. [20] and those for other species were taken from the MINTEQA2 database. Intrinsic stability constants for reactions at carbonate-aqueous solution interface for calcite and magnesite were taken from Ref. [26] (see Section 3.3.1). The activity coefficients of free aqueous ions and charged complexes were calculated using the Davies equation. The activity coefficients of surface species were set equal to 1. For all solids studied, a surface complexation model which assumes constant capacitance of the electric double layer (CCM) was used.

2.5. X-ray absorption spectroscopy

XAFS spectra (including the X-ray absorption near-edge structure region or XANES and the extended X-ray absorption fine-structure region or EXAFS) were collected at ambient conditions (20 ± 2 °C, 1 atm) in the fluorescence mode at the GaK-edge (~10, 370 eV) over the energy range 10,200–11,800 eV on the collaborative research group IF BM 32 beam line at the European Synchrotron Radiation Facility (ESRF, Grenoble, France). The storage ring was operated at 6 GeV with a 200–150 mA current. The beam energy was selected using a Si(111) double crystal monochromator with sagittal focusing. The fluorescence spectra were collected using a Canberra 30-element solid state detector. The samples (wet mineral powders with adsorbed Ga or aqueous solutions) were placed in Teflon cells with two 25-μm Kapton film windows. The spectra acquisition procedure was similar to that described in Refs. [22,27]. Three to six scans (of ~50 min/scan data collection time) for each sample were collected to high-energy values (up to $k \sim 14$ Å^{-1}, where k is the photoelectron momentum). Solid gallium hydroxide (α-GaOOH), nitrate ($Ga(NO_3)_3 \cdot 9H_2O$), and 1–5 mM gallium nitrate in acid (pH 1.1, $Ga(H_2O)_6^{3+}$) and alkaline (pH 9.7, $Ga(OH)_4^-$) aqueous solutions, which can serve as structural models for Ga local environment, were recorded in transmission and fluorescence modes, respectively.

Data analysis was performed with the Athena and Artemis packages [28] based on FEFFIT [29] and FEFF [30] programs. Briefly, energies were recalculated into k-space (Å^{-1}) with E_0 (i.e., the energy where k is zero), arbitrarily chosen at maximum of the main-edge first derivative. Spectra were background subtracted using the AUTOBK algorithm [31], normalized to the absorption-edge step, weighted by k^3, filtered over the k range from ~2.0 to 11–13 Å^{-1} (depending on spectral noise), and Fourier-transformed (Kaiser–Bessel window with dk values of 3.0) to isolate different atomic shells. To obtain structural information, fits were performed in the R-space on both real and imaginary parts of one or several Fourier transform (FT) contributions [29]. This gives the identity of the backscattering atoms (e.g., O, Ga, Ca, Mn), Ga–neighbor distance (R) and coordination number (N), and the Debye–Waller (DW) factor (σ^2) for a given scattering path. In addition to these structural parameters, a single nonstructural parameter, ΔE, was varied in initial fits to account for its estimate made by FEFF. Raw EXAFS spectra were also fitted with multiple shells; they produced values of structural parameters similar to those extracted from fits of FT-filtered signals. For most spectra of our dilute samples which showed weak second shell contributions around Ga and/or significant noise at high k-values, fits of the total EXAFS spectrum were, however, less robust and exhibited larger uncertainties than those for the FT-filtered fits. Consequently, the results of the latter models were considered to be more reliable and they are reported in this study. Typical uncertainties associated with values of R and N for the first atomic shell were ~0.01–0.02 Å and ~20%, respectively. For the second shells they are larger and sometimes attain ±0.07 Å and 50%, respectively (see Table 1).

Theoretical ab initio backscattering amplitude and phase-shift functions for Ga–O, Ga–Ga, Ga–Ca/Mn/Mg/C single and multiple scattering paths were computed using the FEFF 8.0 code [30]. For these calculations, we used the crystal structure of $GaCaO(BO_3)$ [32], which we artificially modified by replacing Ca by Mg (or Mn) and B by C. The amplitude reduction factor (S_0^2) used in modeling of experimental sorption samples was fixed at 1.0 as found by fitting EXAFS spectra of Ga solids and solutions [22]. The influence of anharmonic disorder in determining structural parameters was checked using the cumulant expansion method [33]. The typical values of third- and fourth-order cumulants (C_3 and C_4) found when fitting the filtered signal for the Ga first coordination shell were on the order of $\sim 10^{-5}$–10^{-4} and, consequently, too small to affect R and N values derived from fits without cumulants. The influence of possible multiple scattering (MS) events within the Ga first and second coordination shells on the EXAFS spectra was also tested using the FEFF code, assuming local T_d and O_h geometries around Ga, as found in the model compounds investigated. These contributions were found to be too weak and thus do not affect the EXAFS structural parameters derived for our sorption samples.

In addition to these "classical" EXAFS approaches, wavelet analyses (see Ref. [34] for details) were also performed on selected spectra. The continuous cauchy wavelet transform [34,35] allows more straightforward qualitative interpretations of EXAFS spectra, such as MS features or next-nearest neighbors identification, in particularly, distinguishing light versus heavy neighbors.

3. Results and discussion

3.1. Structures of surface complexes as studied by XAFS

3.1.1. Calcite

Normalized k^3-weighted EXAFS spectra and their corresponding Fourier transforms of three calcite samples with Ga adsorbed from aqueous solutions at initial concentration of 1.0, 0.1, and 0.01 mM and pH ~ 6–7 are shown in Figs. 1A and 1B. All three spectra exhibit first-shell signals from five to six oxygens with Ga–O distances between 1.9 and 2.1 Å. EXAFS modeling shows that the first shell of two more concentrated samples is split into two oxygen subshells with Ga–O distances of 1.93 and 2.09 Å (Table 1). This is demonstrated in Fig. 2, where we compare single- and double-path fits of the first Ga shell for the sample having $[Ga]_0 = 1.0$ mM. Including two O subshells improves the fit quality by a factor of 2. Such first-shell splitting is similar to that observed in Ga oxyhydroxides (e.g., α-GaOOH), where the difference between Ga–O and Ga–OH bond lengths (1.93 and 2.08 Å, respectively, Ref. [36]) induces signifi-

Table 1
Structural parameters of the atomic environment of gallium adsorbed on mineral surfaces at ambient temperature and pressure from 0.01 M $NaNO_3$ solution, pH 6.8 ± 0.3

Sample	k-range ($Å^{-1}$)	R-range (Å)	Edge energy (eV)	Scatterer	N (atoms)	R (Å)	σ^2 ($Å^2$)	ΔE (eV)	R-factor
Aqueous Ga									
5 mM Ga pH 9.7	2.6–13.4	1.2–2.1	10,370.3	Oxygen	4.1 ± 0.3	1.84 ± 0.01	0.0035 ± 0.001	11.0 ± 1.5	0.003
1 mM Ga pH 1.1	2.6–13.2	1.2–2.1	10,371.5	Oxygen	5.9 ± 0.4	1.97 ± 0.01	0.005 ± 0.002	8 ± 2	0.010
Adsorbed Ga									
$CaCO_3$ $[Ga]_0 = 1$ mM $[Ga]_{ads} = 1.6$ μmol/m^2	2.7–13.0	1.2–3.8	10,371.8	Oxygen 1	3.7 ± 0.7	1.93 ± 0.01	0.006 ± 0.002		
				Oxygen 2	1.3 ± 0.5	2.09 ± 0.04	0.006(f)		
				Gallium 1	3.4 ± 1	3.06 ± 0.03	0.01(f)		
				Gallium 2	0.7 ± 0.3	3.51 ± 0.04	0.01(f)	12.3 ± 1.5	0.015
$CaCO_3$ $[Ga]_0 = 0.1$ mM $[Ga]_{ads} = 0.16$ μmol/m^2	2.7–13.0	1.2–3.8	10,372.7	Oxygen 1	4.2 ± 0.7	1.94 ± 0.04	0.006(f)		
				Oxygen 2	1.6 ± 0.7	2.09 ± 0.06	0.006(f)		
				Gallium 1	2.8 ± 0.6	3.07 ± 0.03	0.007(f)		
				Gallium 2	1.6 ± 1.0	3.57 ± 0.04	0.007(f)	11.3 ± 1.5	0.018
$CaCO_3$ $[Ga]_0 = 0.01$ mM $[Ga]_{ads} = 20$ nmol/m^2	2.5–12.5	1.2–2.1	10,372.6	Oxygen	5.0 ± 1.0	1.94 ± 0.01	0.007 ± 0.001	9.2 ± 0.5	0.030
$MgCO_3$ $[Ga]_0 = 0.01$ mM $[Ga]_{ads} = 0.5$ μmol/m^2	2.5–11.0	1.2–2.1	10,371.8	Oxygen 1	5.3 ± 0.5	1.90 ± 0.02	0.008(f)		
				Oxygen 2	1.6 ± 0.5	2.12 ± 0.02	0.008(f)	10 ± 1	0.0011
MnO_2 $[Ga]_0 = 0.01$ mM $[Ga]_{ads} = 0.6$ nmol/m^2	2.5–11.0	1.2–4.0	10,372.0	Oxygen	6.5 ± 1.5	1.91 ± 0.01	0.012 ± 0.004		
				Manganese 1	0.9 ± 0.3	2.98 ± 0.04	0.005(f)		
				Manganese 2	0.6 ± 0.3	3.42 ± 0.07	0.005(f)	7 ± 2	0.011

Note. R = gallium-backscatterer mean distance, N = backscatterer coordination number, σ^2 = squared Debye–Waller factor (relative to $\sigma^2 = 0$ adopted in the calculation of reference amplitude and phase functions by FEFF8); ΔE = nonstructural parameter accounting for phase shift of total EXAFS spectrum between experiment and FEEF calculation; R-factor defines goodness of the total fit in R-space as described in IFEFFIT [29]; (f) = DW factor was varied in initial fits and then fixed at the best value in the final fit.

cant distortions in the GaO_6 octahedron. For the most dilute sample ($[Ga]_0 = 0.01$ mM), no first shell splitting was detected within error: fits with two distinct Ga–O paths always converged to a single path with $R = 1.94 \pm 0.01$ Å and $N = 5 \pm 1$. This might reflect either a lower signal-to-noise ratio of the dilute sample, which limits the exploitable k-range to ∼12 $Å^{-1}$ (see Table 1), or a less distorted Ga atomic environment at lower surface loadings. The derived average Ga–O distance is close to that for the octahedral Ga in gallium oxy(hydr)oxides and acid aqueous solution (1.90–2.10 Å, Refs. [22,37]), and it is significantly higher than that for the tetrahedral Ga in Ga-bearing zeolites and alkaline solutions (1.78–1.85 Å, ([22] and references therein)). Nevertheless, it should be kept in mind that taking account of the relatively low signal-to-noise of our dilute samples and thus the limited k-range investigated, the presence in the first coordination shell of 10–15% of ^{4}Ga with $R \sim 1.8$ Å cannot be completely excluded.

The dominant presence of $^{[6]}$Ga in the three calcite samples investigated is also supported by XANES spectra. The position in energy of the K-edge absorption step ($E_0 \sim 10,372 \pm 0.5$ eV; see Section 2.5 and Table 1) is similar to that observed for the Ga^{3+} aqueous solution and $^{[6]}$Ga solids (Ref. [22]). This energy and the spectral shape are different from those for the tetrahedral Ga environment ($E_0 \sim 10,370 \pm 0.5$ eV).

In contrast to the sample with $[Ga]_0 = 0.01$ mM, the samples with $[Ga]_0 = 1.0$ and 0.1 mM exhibit significant second shell contributions arising from Ga–Ga pairs (Fig. 1, Table 1). Modeling of these features yields two Ga subshells with distances ∼3.05 and ∼3.5 Å. These distances are very similar to those observed for polymeric Ga hydroxide complexes formed in aqueous solution during Ga^{3+} hydrolysis at $2 < pH < 5$ whose structures are composed of $Ga(O,OH,H_2O)_6$ octahedra sharing edges and double corners (see Ref. [22] for details).

The derived Ga–O and Ga–Ga distances and coordination numbers clearly imply the dominant formation of hexacoordinated polymeric oxyhydroxide complexes during the sorption of Ga on calcite surfaces from concentrated (>0.1 mM) aqueous solutions at neutral pH producing high surface loading (i.e., ∼ μmol/m^2). At lower aqueous metal concentration

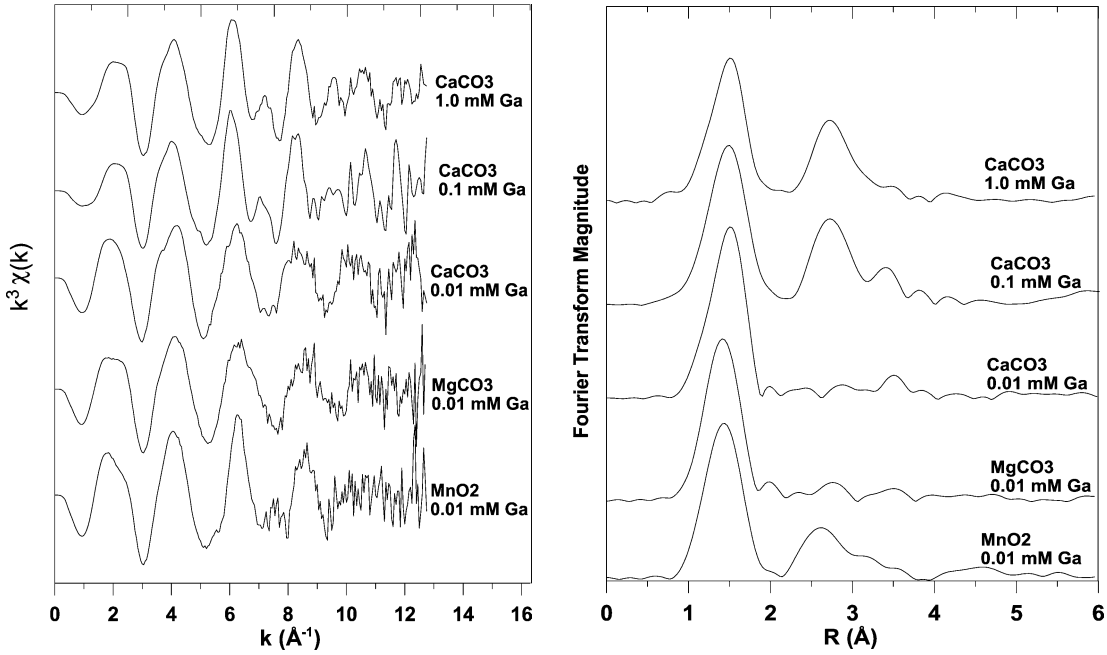

(A) (B)

Fig. 1. (A)Normalized k^3-weighted EXAFS spectra at GaK-edge of selected adsorption samples, and (B) their corresponding Fourier transform magnitudes (not corrected for phase shift).

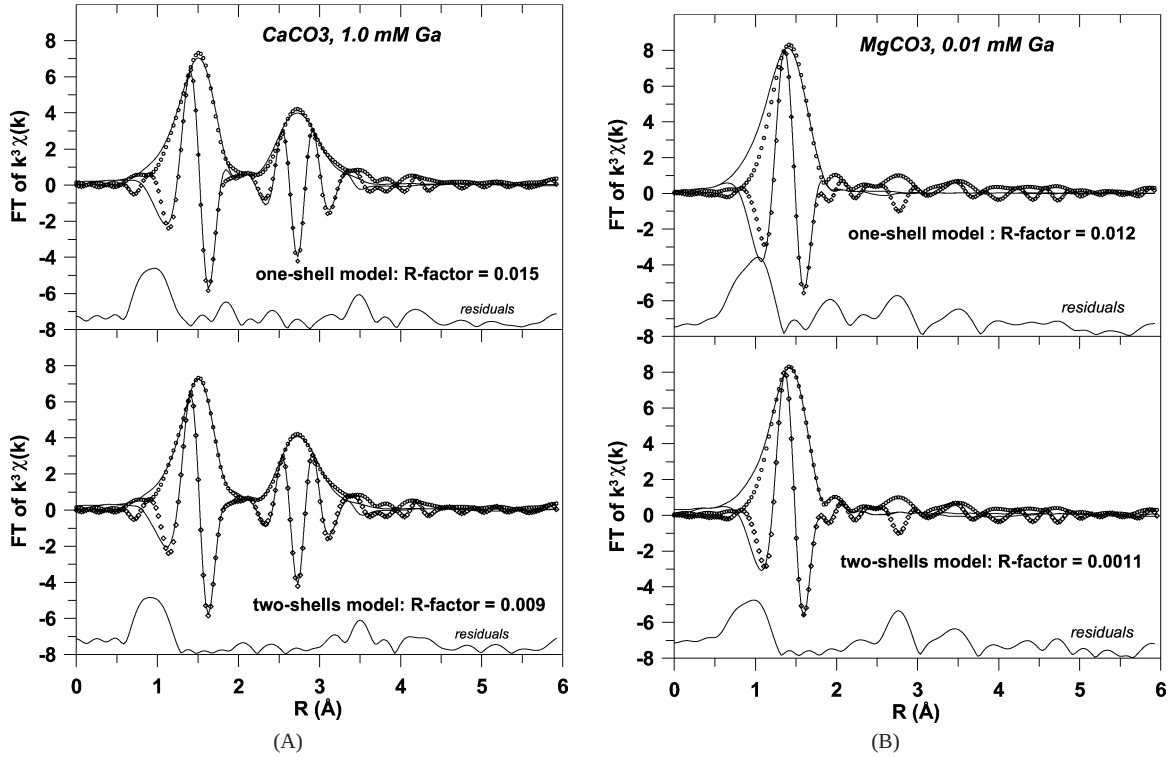

(A) (B)

Fig. 2. Example of EXAFS fitting in R-space for Ga sorbed on (A) $CaCO_3$ and (B) $MgCO_3$ (see Table 1) using one- and two-subshell models for the first Ga–O shell. The points represent the experimental data for FT magnitude and imaginary part of the spectrum and the solid lines stay for the corresponding fits. It can be seen that the use of a two-subshell model improves the fit quality by factors of ∼2 and 10, respectively, for calcite and magnesite samples.

($[Ga]_0 \leqslant 0.01$ mM), no second-shell contribution is detected on the calcite surface, and Ga still remains essentially hexacoordinated. The absence of second-shell EXAFS signal for this dilute sample indicates that no Ga polymers are formed at the surface from such dilute solutions and low surface loadings (i.e., ∼nmol/m^2). The incapability of the EXAFS, which is very sensitive to disorder, to detect Ga–Ca contributions in our samples might reflect a high degree of freedom

and looseness associated with such bonds. The change of the Ga environment from tetrahedra ($Ga(OH)_4^-$) at pH > 5 in solution [20–22] to octahedra at the surface suggests specific interaction with surface sites, i.e., nonelectrostatic covalent adsorption. Therefore, the most plausible scenario for the adsorbed Ga complex is an octahedron sharing one oxygen with the Ca atom on a surface similar to those of the mononuclear inner-sphere complexes of Cu(II) and Zn(II) coordinated to Ca sites at the calcite surface [38]. This is in agreement with the calcite surface structure in aqueous solutions as inferred from numerous spectroscopic (XPS, TOF-SIMS, AFM) observations: the vacant O sites created during cleavage on the Ca octahedra are filled by OH or water and connected to the surface through one bond with Ca [39,40]. X-ray reflectivity measurements at the calcite (104)–water interface confirm the presence of water molecules just above the Ca sites at a height of 2.50 ± 0.12 Å [41], in accord with a molecular dynamics simulation of water adsorbed at the calcite surface with a Ca–O distance of 2.36 Å [42]. Note that the length of the GaO_6 octahedron edge (∼2.9–3.0 Å) is too short to form stable double-corner bonds with the apical oxygens of two adjacent CaO_6 octahedra (Ca–Ca interatomic distances on the dominant (1014) planes of calcite = 4.05 Å). This is in contrast with the adsorption of large divalent cations (e.g., Cd^{2+}, Pb^{2+}) which are known to form double corner linkages (^{2}C-type) with Me–oxygen sites on mineral surfaces [43].

3.1.2. Magnesite

The shape and energy position of the XANES spectrum of Ga sorbed at magnesite from 0.01 mM solution at 0.5 µmol/m^2 surface coverage ($E_0 \sim 10,372$ eV) is close to that for the calcite samples and octahedral Ga in solids and acid solution, thus suggesting similar Ga coordination. Indeed, EXAFS spectrum of this sample exhibits a single first shell contribution arising from ∼6 oxygen atoms (Fig. 1). This shell is found to be split into two subshells with $R_1 = 1.9$ Å, $N_1 = 5.3$, and $R_2 = 2.12$ Å, $N_2 = 1.6$ (Table 1). Note that such a double-shell fit improves the fit quality by a factor of 10 in comparison with a single-shell fit (Fig. 2). It is thus can be concluded from these limited EXAFS data that Ga sorbs on $MgCO_3$ surface either as a strongly distorted octahedral complex having different bond lengths with the surface oxygens and OH/H_2O groups in solution (Section 3.3.1), or as two different types of octahedral complexes with relative percentages of ∼70–80 and ∼30–20%. However, more data at different concentrations are needed to resolve this issue.

3.1.3. Manganese dioxide

Similar to the XANES spectra of other sorbed samples, the spectrum of MnO_2 sample with Ga sorbed from an aqueous solution at $[Ga]_0 = 0.012$ mM Ga and pH 6.8 exhibits shape and energy position typical of an octahedral Ga coordination (Table 1). The EXAFS spectrum shows two distinct contributions arising from first Ga–O and second Ga–(Mn or/and Ga) atomic shells, respectively (Fig. 1). Modeling shows that the first shell corresponds to GaO_6 octahedra with an average Ga–O distance of 1.91 Å with a relatively high DW factor (∼0.01), which might indicate significant distortions of the Ga octahedron (Table 1). However, no first-shell splitting could be detected in the limit of the spectral resolution.

EXAFS fits of the second shell were much less robust because of the short exploitable k-range (2.5–11 Å^{-1}) for this dilute sample (Fig. 1) and the possibility of presence of multiple (Mn, Ga) subshells. To better identify the second shell neighbors, we used the continuous Cauchy wavelet transform (CCWT) of this spectrum [34]. Comparison of EXAFS spectra (Fig. 1), FT imaginary parts, and CCWT modulus (not shown) of gallium sorbed on MnO_2 from 0.012 mM solution and gallium sorbed on $CaCO_3$ from 1.0 mM solution with surface loadings of 0.6 nmol/m^2 and 1.6 µmol/m^2, respectively, revealed that the maximum of the second-shell amplitude for the MnO_2 sample is shifted to lower k-values ($k_{max} \sim 7.0$ Å^{-1}) in comparison to that of the second shell of the $CaCO_3$ sample ($k_{max} \sim 7.5$–8.0 Å^{-1}), in which Ga–Ga contributions were unambiguously identified (Section 3.1.1). Because the EXAFS amplitude term for Mn backscatterers is indeed shifted to k-values lower than that for a heavier Ga backscatterer (see Ref. [34] for details), it is very likely that the Ga atoms in the MnO_2 sample are surrounded by Mn rather than Ga neighbors. This is also in agreement with the very low surface coverage (i.e., <0.01% of total site number) of Ga in MnO_2 sample.

Based on the analysis above, the second shell of the MnO_2 sample was reasonably modeled with two Ga–Mn contributions at ∼ 3.0 and ∼3.4 Å, respectively (Table 1). Despite the high uncertainties associated with R and N values derived for the second shell, it can be concluded that Ga sorbs on MnO_2 surface as hexacoordinated inner-sphere complexes that share edges (monodentate) and double corners (bidentate) with MnO_6 octahedra. These structures are similar to those found using XAFS spectroscopy for divalent metal cations (Zn^{2+}, Cd^{2+}) adsorbed onto or co-precipitated with Mn oxides and oxyhydroxides [44–46]. Other XAFS studies indicate, however, that some cations (e.g., Zn^{2+}, Ni^{2+}, Sr^{2+}, [47,48]) can form outer-sphere complexes with hydrous Mn oxide surfaces. These differences might be related to the extreme variability of Mn (hydr)oxide phases and their surface properties, and the mode of metal uptake (adsorption versus co-precipitation).

3.2. Results from batch adsorption

Adsorption of Ga on calcite was studied as a function of pH, $[Ga]_0$, $[Ca^{2+}]_t$, and [Alk]. For other minerals, only the effect of pH at constant initial Ga concentration (pH-dependent adsorption edge) was investigated.

The percentage of adsorbed gallium on calcite is plotted as a function of pH in Fig. 3 for three ranges of Ga concentration: 0.1–0.5 mM (A), 12–24 µM (B), and 14 nM (C).

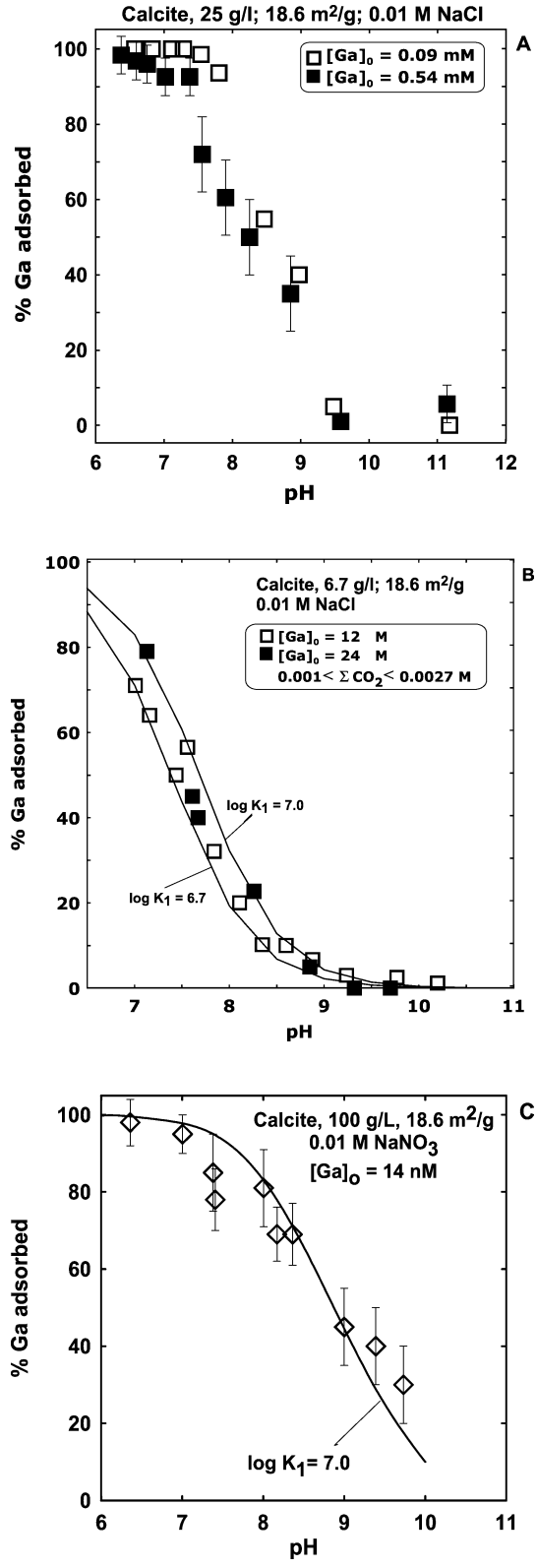

Fig. 3. Effect of pH on Ga adsorption on calcite. (A) Experiments at $[Ga]_0 = 5.4 \times 10^{-4}$ M (solid squares) and 9.0×10^{-5} M (open squares). (B) Experiments at $[Ga]_0 = 24 \times 10^{-5}$ M (solid squares) and 12×10^{-5} M (open squares); solid lines were calculated using SCM generated in this study with $\log K_1 = 7.0$ and 6.7, respectively. (C) Experiments at $[Ga]_0 = 14$ nM; solid line was calculated using SCM generated in this study with $\log K_1 = 7.0$.

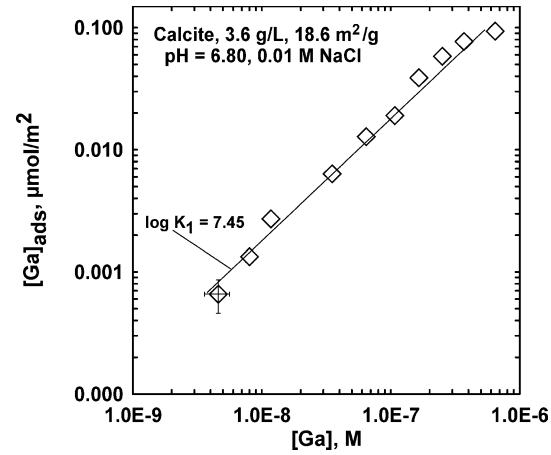

Fig. 4. Gallium adsorption isotherm on calcite obtained in 0.01 M NaCl at pH 6.8. The solid line was calculated using SCM generated in this study with $\log K_1 = 7.45 \pm 0.05$.

Adsorption of Ga on calcite is highest at pH below 7 and decreases with pH at $7 \leqslant \text{pH} \leqslant 10$ for the whole range of Ga concentrations investigated in this study. It can be seen from these figures that the same pH dependence is observed for solutions undersaturated with respect to Ga oxy(hydr)oxides (Fig. 3C, $[Ga]_0 = 14$ nM) and those supersaturated with respect to α-GaOOH at pH < 8 (Fig. 3B, $[Ga]_0 = 0.01$–0.024 mM). Therefore, we suggest the absence of individual Ga solid phases precipitation in solutions supersaturated with respect to α-GaOOH at pH from 7 to 8. This was also confirmed by the stability of Ga concentration in blank experiments performed in this pH range without solid phase (Section 2.2). However, for samples having $[Ga]_0 = 0.024$ mM, some degree of surface precipitation or polymerization of adsorbed Ga is possible, as follows from the EXAFS analysis (Section 3.1.1, Table 1).

The concentration of adsorbed Ga as a function of equilibrium Ga concentration in solution at pH 6.80 (Langmurian adsorption isotherm) is presented in Fig. 4. The value of maximum adsorption can be estimated as $\geqslant 0.1$ μmol/m^2 at pH 6.8, which is comparable with other anion adsorption densities on calcite: ∼0.2 μmol/m^2 for selenite [49]; 0.3–0.8 μmol/m^2 for phosphate [50,51]. It can be seen from Fig. 4 that the adsorption density increases with a slope of 1 with respect to [Ga] indicating a 1:1 stoichiometric interaction between Ga ions in solution and the surface adsorption sites [52].

The effect of other components of solution, i.e., Ca^{2+} and HCO_3^- ions, has been studied in solutions enriched in $CaCl_2$ and $NaHCO_3$. Results of Ga adsorption at variable solution composition are presented in Table 2. Our experimental setup did not allow varying independently all four parameters of the carbonate system, [Ca^{2+}], [HCO_3^-], [CO_3^{2-}], and pH, and rigorously separating the effect of pH from that of (bi)carbonate and calcium ions. It can be seen from Table 2 that, in accord with our previous findings and results on anion adsorption on calcite [49], the adsorption decreases when

Table 2
Results of Ga adsorption on calcite at various pH, [Alk], and $[Ca]_{tot}$ and surface complexation model prediction of the adsorption

pH	[Alk] (M)	$[Ca]_{tot}$ (M)	% Ga adsorbed (experiment)	% Ga adsorbed (model)
7.32	3.62×10^{-4}	0.01103	40.1	40.8
7.46	4.55×10^{-4}	0.0055	27.5	32.7
7.58	6.10×10^{-4}	0.00229	25.2	26
7.71	8.27×10^{-4}	0.00153	19.9	19.6
7.88	0.00133	9.39×10^{-4}	30.4	26.8
7.98	0.00157	5.54×10^{-4}	25.5	24.7
8.08	0.00309	2.51×10^{-4}	18.6	17.2
8.07	0.00472	1.89×10^{-4}	20.3	16.4
8.15	0.00802	1.16×10^{-4}	17.4	12.3
8.21	0.0117	7.92×10^{-5}	13.9	9.7
8.33	0.0212	4.64×10^{-5}	10.1	5.9

Experimental conditions: 67 m^2/l $CaCO_3$, 0.01 M $NaNO_3$, $[Ga]_0 = 10^{-7}$ M.

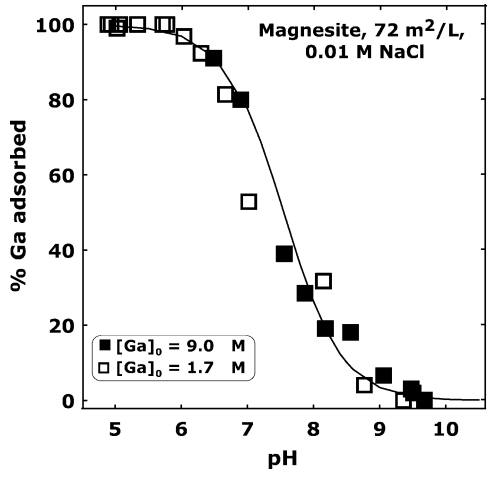

Fig. 5. Effect of pH on Ga adsorption on magnesite at $[Ga]_0 = 9$ μM (solid squares) and 1.7 μM (open squares). The solid line was calculated using SCM generated in this study with $\log K_1 = 5.7 \pm 0.1$.

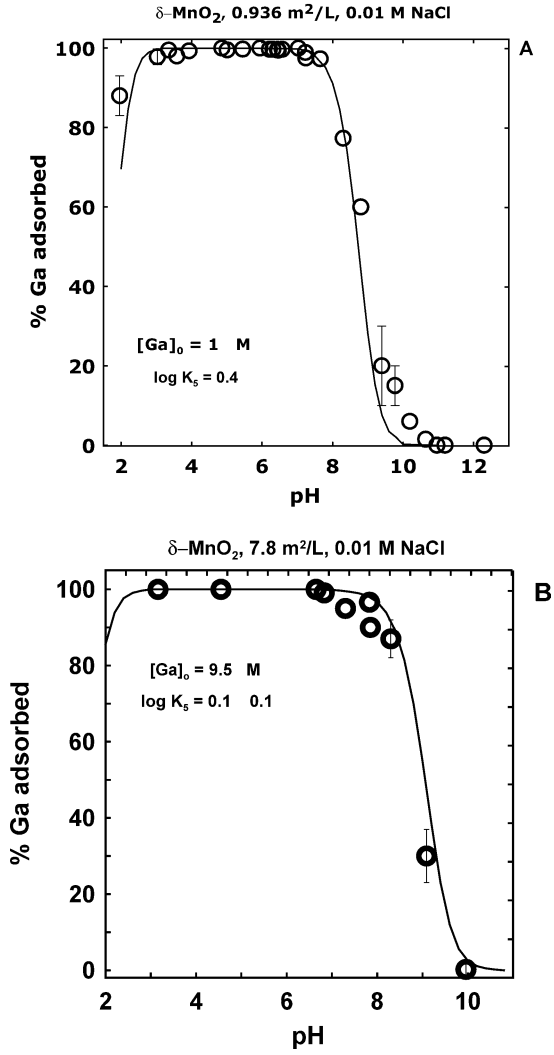

Fig. 6. Effect of pH on Ga adsorption on birnessite at low (A) and high (B) surface concentration in solution. The symbols represent the experimental data and the solid lines were calculated using SCM generated in this study with $\log K_5 = 0.4$ (A) and 0.1 (B).

pH increases from 7 to 8. This tendency is met at a wide range of $[Ca]_{tot}$ and [Alk].

Gallium adsorption on magnesite is very similar to that on calcite (Fig. 5). For two different Ga concentrations in solution, a decrease of the adsorbed amount starts at pH 6, and no adsorption occurs at pH > 9. Adsorption edge of Ga on manganese oxide is presented in Fig. 6: the adsorption is high at $2 < \text{pH} \leqslant 8$ but drops to almost zero at pH ∼ 10. This dependence was observed at two different oxide surface concentrations with 10-fold different initial Ga concentrations. Gallium adsorption on amorphous silica exhibits a contrasting behavior as compared to carbonates: the adsorption edge starts at $\text{pH} \geqslant 2$, and 100% adsorption occurs at $3 < \text{pH} < 10.5$ (Fig. 7).

3.3. Surface complexation modeling

3.3.1. Carbonates

The thermodynamic model for the carbonates–solution interface used in this study [23,26,53–56] postulates the for-

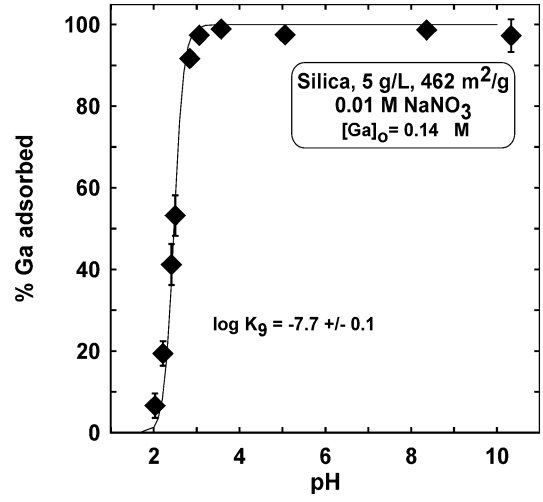

Fig. 7. Effect of pH on Ga adsorption on amorphous silica. The symbols represent the experimental data and the solid line was calculated using SCM generated in this study with $\log K_9 = -7.7 \pm 0.1$.

mation of two primary protonation sites, $>MeOH^0$ (Me = Ca or Mg) and $>CO_3H^0$, having a 1:1 stoichiometry on the surface. In this model, the initial sites left by cleavage on the surface are assigned a +1 or −1 charge. This originates from the assumption that a half of the Me^{2+} and CO_3^{2-} bonds on the surface is satisfied with underlaying bulk oxygens resulting in $>Me^{1+}$ and $>CO_3^{1-}$ initial species exposed on the surface plane. Subsequent hydration and adsorption of constituent ions from solution lead to the formation of the following surface species: $>CO_3H^0$, $>CO_3^-$, $>CO_3Me^+$, $>MeOH^0$, $>MeO^-$, $>MeOH_2^+$, $>MeHCO_3^0$, and $MeCO_3^-$. The constants of surface reactions, surface site densities for calcite and magnesite, and electrical double-layer capacitances used in this study are taken from Ref. [26].

It follows from the results of our adsorption experiments that Ga adsorbs on the calcite surface as an anion. The most likely atomic structure, though it is not fully derived from the EXAFS measurements, implies the adsorption of six-coordinated Ga on single hydrated metal site, $>MeOH_2^+$, sharing one oxygen atom with the surface Me and undergoing protonation/deprotonation reactions: $>Me–O–Ga(OH)_n(H_2O)_{5-n}^{2-n}$. Because EXAFS is not capable of seeing hydrogen, the n value (protonation degree of the surface complex) has been determined by fitting the experimental pH dependence of Ga adsorption on calcite and magnesite. Only the stoichiometry $n = 1$ was able to reproduce the experimental results; both $n = 0$ and $n = -1$ failed. In terms of basic thermodynamic species, the adsorption of Ga on the carbonate surface can, therefore, be represented as

$$>MeOH^0 + Ga^{3+} + 5H_2O \Rightarrow Me–H_9GaO_6^+ + 2H^+. \quad (1)$$

Because at pH higher than 7, $>MeOH_2^+$ (surface) and $Ga(OH)_4^-$(aq) are the dominant species in the system, the adsorption reaction can be written as

$$>MeOH_2^+ + Ga(OH)_4^- + 2H_2O \Rightarrow Me–H_9GaO_6^+ + OH^- \quad (2)$$

which assumes the decrease of adsorption with pH as observed in the experiments (Figs. 3B, 3C, and 5). The surface complex thus formed can be schematically represented as

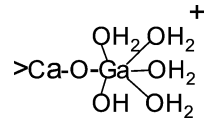

which suggests the presence of four water molecules, one hydroxyl group and one common oxygen with the surface Ca or Mg atom. However, in view of the lack of evidences for Ga–Ca contributions in the EXAFS spectra, this structure and exact stoichiometry of reactions (1) and (2) with respect to $>MeOH^0$ can be considered as a first approximation, amenable to further refinement.

Surface complexation model predictions of Ga adsorption on calcite and magnesite are represented as solid lines in Figs. 3–5 and the surface reactions together with their intrinsic stability constants are given in Table 3. In this modeling, only one adjustable parameter, the intrinsic stability constant of reaction (1), was used. All acid–base and Me^{2+}, $CO_3^{2-}HCO_3^-$ adsorption reaction constants, site densities, and EDL capacitance [26] were fixed during the fit. This allows to estimate the reaction (1) stability constant as $\log K_1 = 7.0 \pm 0.3$ for calcite. It can be seen in Figs. 3B and 3C that, within the experimental uncertainty, the same value of this constant is necessary to reproduce the experimental data for a wide range of Ga concentration, i.e., from 14 nM to 24 μM. At higher Ga concentrations in solution, surface polymers or precipitates were detected (Section 3.1.1), and, therefore, surface complexation modeling of these results is not possible.

Experiments at variable [Ca] and [Alk] were specially designed to test the effect of solution constituents on Ga adsorption (Table 2). Because gallium adsorbs as an anion, it is possible that a competition with HCO_3^- and CO_3^{2-} for $>CaOH_2^+$ sites occurs. The surface complexation model elaborated in this study is capable of predicting this behavior: the last column in Table 2 was calculated using parameters of SCM for calcite [26], taking into account the carbonate, bicarbonate, and calcium ion adsorption and only $\log K_1$ as an adjustable parameter. The values of $\log K_1$ determined from these data (i.e., 6.6 and 7.0) fall within the range obtained from adsorption edge and adsorption isotherm modeling (Figs. 3 and 4). Within the context of surface complexa-

Table 3
Surface reactions for Ga adsorption on mineral surfaces and their intrinsic stability constants

Solid	Surface reaction	$\log K^0_{int}$ (298.15 K, $I = 0$)
Calcite	(1) $>CaOH^0 + Ga^{3+} + 5H_2O \Rightarrow Ca–H_9GaO_6^+ + 2H^+$	$7.0 \pm 0.3 - 3.19$
	(2) $>CaOH_2^+ + Ga(OH)_4^- + 2H_2O \Rightarrow Ca–H_9GaO_6^+ + OH^-$	
Magnesite	(1) $>MgOH^0 + Ga^{3+} + 5H_2O \Rightarrow Mg–H_9GaO_6^+ + 2H^+$	$5.7 \pm 0.3 - 3.24$
	(2) $>MgOH_2^+ + Ga(OH)_4^- + 2H_2O \Rightarrow Mg–H_9GaO_6^+ + OH^-$	
δ-MnO_2	(5) $>MnOH^0 + Ga^{3+} + 5H_2O \Rightarrow Mn–H_8GaO_6^0 + 3H^+$	0.25 ± 0.15
	(6) $>2MnOH^0 + Ga^{3+} + 4H_2O \Rightarrow Mn_2–H_7GaO_6^0 + 3H^+$	4.1 ± 0.1
SiO_2	(9) $>SiOH^0 + Ga^{3+} + 3H_2O \Rightarrow SiO–Ga(OH)_3^- + 4H^+$	-7.7 ± 0.1

tion model, the decrease of $Ga(OH)_4^-$ adsorption with [Alk] increase at pH $\geqslant$ 8 is due to the change of dominant surface species from $>CaOH_2^+$ to $>CaHCO_3^0$, $>CaCO_3^-$, and $>CaOH^0$.

The logarithm of intrinsic stability constant of reaction (1) for magnesite was found to be 5.7 ± 0.1. The difference from the corresponding value for calcite does not reflect the different affinity of Ga to the surfaces of these two carbonates. Rather, it corresponds to different acid–base properties of metal surface centers for calcite and magnesite [26]. Indeed, logarithms of reaction (2) stability constants are equal to -3.19 for calcite and -3.24 for magnesite (Table 3), suggesting the similarity of $Ga(OH)_4^-$ adsorption on hydrated surface centers $>MeOH_2^+$.

3.3.2. Mn(IV) oxide

It follows from the results of XAFS measurements that the adsorbed complex contains six oxygens at 1.91 Å in the first coordination sphere of Ga. Because the protonation of the complex and its charge cannot be directly inferred from XAFS spectroscopy, we used the adsorption data to determine the stoichiometry of adsorption reaction with respect to H^+(aq). Gallium adsorption on manganese dioxide was modeled within the 2-pK constant capacitance model (CCM). Surface site density was set to 16 µmol/m^2, EDL capacitance to 1 F/m^2, and intrinsic surface stability constants for reactions

$$>MnOH^0 + H^+ \Rightarrow MnOH_2^+, \quad (3)$$

$$>MnOH^0 - H^+ \Rightarrow MnO^-, \quad (4)$$

were fixed as $\log K_3 = -0.2$ and $\log K_4 = 7.5$ [57]. Only one adjustable parameter, the stability constant for reaction of Ga adsorption in the form of the monodentate mononuclear complex

$$>MnOH^0 + Ga^{3+} + 5H_2O \Rightarrow Mn\text{–}H_8GaO_6^0 + 3H^+ \quad (5)$$

was varied to reproduce the experimental data (solid lines in Fig. 6). Between two independent sets of experiments, a reasonable agreement was found using $\log K_5 = 0.25 \pm 0.15$ (Table 3). Neither +1 nor −1 charged complexes allowed to reproduce the experimental adsorption edge in the whole range of pH studied. According to the first possible scenario, the tentative structure of mononuclear complex formed can be represented as

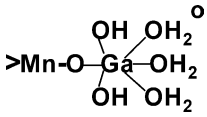

With such a stoichiometry, the desorption of $Ga(OH)_4^-$(aq) from manganese dioxide at pH > 8 is likely to be related to the change of surface species from $>MnOH^0$ to charged $>MnO^-$ at pH $\geqslant$ 7.5 ($\log K_4 = 7.5$) and the electrostatic repulsion of two dominant negatively charged species. The value of $\log K_5$ recommended in this study depends on the choice of SCM parameters for manganese dioxide. For example, the use of surface complexation model for δ-MnO_2 with $\log K_3 = -1.6$, $\log K_4 = 6.2$ [58] provided equally good fit to the data with $\log K_5 = 1.35 \pm 0.15$.

It follows from the results of EXAFS study that Ga can also interact with the surface of manganese dioxide forming two types of complexes, monodentate and bidentate sharing the edges and corners with MnO_6 octahedra. However, the EXAFS is not capable quantifying the relative proportion of two complexes. Therefore, this second scenario was tested by modifying the adsorption reaction (5) to

$$>2MnOH^0 + Ga^{3+} + 4H_2O \Rightarrow >Mn_2\text{–}H_7GaO_6^0 + 3H^+ \quad (6)$$

implying a bidentate binuclear surface complex:

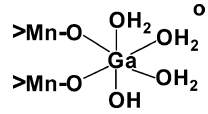

A close description of the experimental pH-dependent adsorption edge was achieved with $\log K_6 = 4.1 \pm 0.1$ (the solid lines corresponding to fits with K_5 and K_6 in Fig. 6 are undistinguishable). Therefore, the thermodynamic approach used in this study, though capable of determining the charge and protonation degree of the surface complex, is unable to resolve its stoichiometry with respect to surface centers and thus further study is necessary. It is worth noting that the triple-layer model (TLM) of Ga(III) adsorption on Al_2O_3 [18] provided equally good fits to the data within the concept of bidentate or monodentate surface complexes.

3.3.3. Amorphous silica

Adsorption of Ga on amorphous silica was modeled with a 2-pKa CCM with 10 µmol/m^2 of surface sites assuming two surface reactions responsible for the amphoteric properties of silica,

$$>SiOH^0 + H^+ \Rightarrow SiOH_2^+, \quad (7)$$

$$>SiOH^0 - H^+ \Rightarrow SiO^-, \quad (8)$$

with $\log K_7 = -3.0$ and $\log K_8 = -7.0$. These parameters are consistent with CCM for SiO_2 [57] and recent spectroscopic observations of quartz surfaces [59]. The intrinsic surface stability constant of Ga adsorption reaction on silica,

$$>SiOH^0 + Ga^{3+} + 3H_2O \Rightarrow SiO\text{–}Ga(OH)_3^- + 4H^+, \quad (9)$$

was used as the only adjustable parameter to reproduce the pH-dependent adsorption edge (Table 3). The value of $\log K_9 = -7.7 \pm 0.1$ determined from the pH-dependent adsorption edge was used to generate the solid line in Fig. 7. Fitting the experimental data with a surface complex of another stoichiometry (i.e., charge of zero or +1) was not successful. Unfortunately, the structure and stoichiometry of surface complexes formed by Ga adsorption on silica were not tested by XAFS spectroscopy. However, by analogy with Ga and Al complexation with silica in aqueous solution [22,

60,61] one can hypothesize that in neutral and basic Si-bearing solutions Ga adsorbs in a tetrahedral atomic environment with oxygens such that $Ga(O,OH)_4$ is attached to one or two silicate groups on the surface. The enhanced stability of tetrahedral Ga over a wide range of pH in the presence of dissolved silicate ions has been recently demonstrated by NMR and XAFS techniques [22]. It is very likely therefore that this tetrahedral coordination dominates the speciation of adsorbed Ga in a very wide range of pH.

4. Concluding remarks

This study allowed first-order understanding of Ga interactions with surfaces of carbonate and oxide minerals in aqueous solution by combining traditional macroscopic adsorption measurements with in situ XAFS characterization of surface complexes formed. A surface complexation model recently developed for carbonates [26] was found to be a powerful tool for describing Ga adsorption on calcite and magnesite surfaces using only one adjustable parameter, the reaction constant of $Ga(OH)_4^-(aq)$ with $>MeOH_2^+$ surface groups. At neutral to alkaline pH, gallium changes its coordination from tetrahedrally coordinated $Ga(OH)_4^-$ anion in solution to the hexacoordinated $Ga(O,OH,H_2O)_6$ on the surface where it is likely to be bound to the metal center via octahedral corners. It is thus possible that the dominance of acid moieties on the carbonate surface ($>MeOH_2^+$) which provide extra amount of protons in comparison to the bulk aqueous solution, favorizes the change of Ga atomic coordination from 4 to 6 when adsorbing from solution on a mineral surface. This is consistent with the known versatility of Ga to change its coordination during Ga^{3+} hydrolysis in aqueous solution and in mineral phases [22]. Because the EXAFS is not capable of seeing hydrogen, the protonation state of surface complexes can be determined by fitting the macroscopic pH-dependent adsorption edge using a surface complexation approach. Coordination of Ga(III) to deprotonated surface sites forming monodentate (carbonates) or bidentate (manganese oxide) $>(SO)_k{-}Ga(OH)_n(H_2O)_m^{2-n}$ surface complexes (S = Ca, Mg, Mn, or Si) proposed in this study is in accord with a two-step mechanism of Ga(III) and In(III) sorption on γ-Al_2O_3 revealed by pressure-jump techniques [18]: -proton release from surface hydroxyl group(s) followed by coordination of Ga(III)/In(III) species to the deprotonated site(s). In the case of two possible surface complexes present (δ-MnO_2), rigorous quantitative resolution of their relative proportion at the surface requires a special study.

The similarity of Ga and Al hydrolysis and interactions with ligands in aqueous solution allows using results of this study for predicting the interaction of aqueous aluminum with carbonate and oxide mineral surfaces and quantifying the control they exert on aluminum migration in natural waters. It follows from the results of this study that in the pH region of soil solutions and surficial waters (i.e., from 4 to 9), the essential part of inorganic aluminum will be adsorbed on mineral surfaces. Therefore, aluminum migration in the form of suspended solids and soil particles is an important issue which should be taken into account when analyzing Al transport and bioavailability in surficial aquatic environments.

References

[1] J. Gaillardet, B. Dupré, J. Viers, in: H.D. Holland, K.K. Turekian (Eds.), Treatise on Geochemistry, Surface and Ground Water, Weathering, and Soils, vol. 5, Elsevier, Amsterdam, 2003.
[2] B. Dupré, J. Viers, J.-L. Dandurand, M. Polvé, P. Bénézeth, Ph. Vervier, J.-J. Braun, Chem. Geol. 160 (1999) 63.
[3] O.S. Pokrovsky, J. Schott, Chem. Geol. 190 (2002) 141.
[4] O.S. Pokrovsky, B. Dupré, J. Schott, Aquatic Geochem. (2004), in press.
[5] J. Viers, B. Dupré, M. Polvé, J. Schott, J.-L. Dandurand, J.-J. Braun, Chem. Geol. 140 (1997) 181.
[6] D.A. Dzombak, F.M. Morel, Surface Complexation Modeling: Hydrous Ferric Oxide, Wiley, New York, 1990.
[7] M. Kosmulski, J. Colloid Interface Sci. 195 (1997) 395.
[8] M. Kosmulski, J. Colloid Interface Sci. 190 (1997) 212.
[9] A. Manceau, M. Schlegel, K.L. Nagy, L. Charlet, J. Colloid Interface Sci. 220 (1999) 181.
[10] N. Marmier, A. Delisée, F. Fromage, J. Colloid Interface Sci. 212 (1999) 228.
[11] Ch. Tiffreau, J. Lützenkirchen, Ph. Behra, J. Colloid Interface Sci. 172 (1995) 82.
[12] P.M. Schosseler, B. Wehrli, A. Schweiger, Geochim. Cosmochim. Acta 63 (1999) 1955.
[13] Th. Stumpf, A. Bauer, F. Coppin, J.I. Kim, Environ. Sci. Technol. 35 (2001) 3691.
[14] Th. Stumpf, Th. Fanghänel, J. Colloid Interface Sci. 249 (2002) 119.
[15] Th. Stumpf, Th. Rabung, R. Klenze, H. Geckeis, J.I. Kim, J. Colloid Interface Sci. 238 (2001) 219.
[16] K.-S. Chang, C.-F. Lin, D.-Y. Lee, S.-L. Lo, T.J. Yasunaga, Colloid Interface Sci. 165 (1994) 169.
[17] R. Iller, The Chemistry of Silica, Wiley, New York, 1979, pp. 673–676.
[18] C.-F. Lin, K.-S. Chang, C.-W. Tsay, D.-Y. Lee, S.-L. Lo, T. Yasunaga, J. Colloid Interface Sci. 188 (1997) 201.
[19] B. Wehrli, S. Ibric, W. Stumm, Colloids Surf. 51 (1990) 77.
[20] P. Bénézeth, I.I. Diakonov, G.S. Pokrovski, J.-L. Dandurand, J. Schott, I.L. Khodakovsky, Geochim. Cosmochim. Acta 61 (1997) 1345.
[21] I.L. Diakonov, G.S. Pokrovski, P. Bénézeth, J. Schott, J.-L. Dandurand, J. Escalier, Geochim. Cosmochim. Acta 61 (1997) 1333.
[22] G.S. Pokrovski, J. Schott, J.-L. Hazemann, F. Farges, O.S. Pokrovsky, Geochim. Cosmochim. Acta 66 (2002) 4203.
[23] O.S. Pokrovsky, J. Schott, F. Thomas, Geochim. Cosmochim. Acta 63 (1999) 863.
[24] O.S. Pokrovsky, V.S. Savenko, Geochem. Int. 32 (1995) 138.
[25] J.D. Allison, D.S. Brown, K.J. Novo-Gradac, MINTEQA2/PRODEFA2, A Geochemical Assessment Model for Environmental Systems: Version 3.0 User's Manual; USEPA, Athens, GA, 1991.
[26] O.S. Pokrovsky, J. Schott, Environ. Sci. Technol. 36 (2002) 426.
[27] G.S. Pokrovski, J. Schott, F. Farges, J.-L. Hazemann, Geochim. Cosmochim. Acta 67 (2003) 3559.
[28] B. Ravel, EXAFS Analysis Software Using IFEFFIT, available at: http://feff.phys.washington.edu/~ravel/software/exafs/, 2003.
[29] M. Newville, J. Synchrotron Rad. 8 (2001) 322.
[30] A.L. Ankudinov, B. Ravel, J.J. Rehr, S.D. Conradson, Phys. Rev. B 58 (1998) 7565.

[31] M. Newville, P. Livins, Y. Yacoby, E.A. Stern, J.J. Rehr, Phys. Rev. B 47 (1993) 14,126.
[32] Z. Yang, J.K. Liang, X.L. Chen, T. Xu, Y.P. Xu, J. Alloys Compd. 327 (2001) 215.
[33] E.D. Crosier, J.J. Rehr, R. Ingalls, in: D.C. Koningsberger, R. Prins (Eds.), X-Ray Absorption: Principles, Applications, Techniques of EXAFS, SEXAFS and XANES, Wiley–Interscience, New York, 1988, p. 373.
[34] M. Munoz, P. Argoul, F. Farges, Am. Mineral. 88 (2003) 694.
[35] F. Farges, Wavelet Transform of XAFS Spectra, available at: http://www.univ-mlv.fr/~farges/wav/, 2003.
[36] M.F. Pye, J.J. Birtill, P.G. Dickens, Acta Crystallogr. Sect. B 33 (1977) 3224.
[37] L.J. Michot, E. Mantargès-Pelletier, B.S. Lartiges, J.-B. d'Espinose de la Caillerie, V. Briois, J. Am. Chem. Soc. 122 (2000) 6048.
[38] E.J. Elzinga, R.J. Reeder, Geochim. Cosmochim. Acta 66 (2002) 3943.
[39] S.L.S. Stipp, Geochim. Cosmochim. Acta 63 (1999) 3121.
[40] S.L.S. Stipp, C.M. Eggleston, B.S. Nielsen, Geochim. Cosmochim. Acta 58 (1994) 3023.
[41] P. Fenter, P. Geissbühler, E. DiMasi, G. Srajer, L.B. Sorensen, N.C. Sturchio, Geochim. Cosmochim. Acta 64 (2000) 1221.
[42] N.H. de Leeuw, S.C. Parker, J. Chem. Soc. Faraday Trans. 93 (1997) 467.
[43] S.R. Randall, D.M. Sherman, K.V. Ragnarsdottir, C.R. Collins, Geochim. Cosmochim. Acta 63 (1999) 2971.
[44] L. Bochatay, P. Persson, S. Sjöberg, J. Colloid Interface Sci. 229 (2000) 584.
[45] L. Bochatay, P. Persson, J. Colloid Interface Sci. 229 (2000) 593.
[46] S.R. Randal, D.M. Sherman, K.V. Ragnarsdottir, Chem. Geol. 151 (1998) 95.
[47] P. Trivedi, L. Axe, T.A. Tyson, Environ. Sci. Technol. 35 (2001) 4515.
[48] L. Axe, T.A. Tyson, P. Trivedi, J. Colloid Interface Sci. 224 (2000) 408.
[49] Ch.E. Cowan, J.M. Zachara, Ch.T. Resch, Geochim. Cosmochim. Acta 54 (1990) 2223.
[50] R.A. Griffin, J.J. Jurinak, Soil Sci. Soc. Am. Proc. 38 (1974) 75.
[51] W.A. House, L. Donaldson, J. Colloid Interface Sci. 112 (1986) 309.
[52] W. Stumm, Chemistry at the Solid–Water Interface, Wiley, New York, 1992.
[53] O.S. Pokrovsky, J.A. Mielczarski, O. Barres, J. Schott, Langmuir 16 (2000) 2677.
[54] O.S. Pokrovsky, J. Schott, J. Mielczarski, in: Encyclopedia of Surface and Colloid Science, Dekker, 2002, p. 5081.
[55] Ph. Van Cappellen, L. Charlet, W. Stumm, P.A. Wersin, Geochim. Cosmochim. Acta 57 (1993) 3505.
[56] L. Charlet, P. Wersin, W. Stumm, Geochim. Cosmochim. Acta 54 (1990) 2329.
[57] D.A. Sverjensky, N. Sahai, Geochim. Cosmochim. Acta 60 (1996) 3773.
[58] D.A. Kulik, M. Kersten, Mineral. Mag. A 62 (1998) 826.
[59] Y. Duval, J.A. Mielczarski, O.S. Pokrovsky, E. Mielczarski, J.J. Ehrhardt, J. Phys. Chem. B 106 (2002) 2937.
[60] G.S. Pokrovski, J. Schott, J.-C. Harrichoury, A.S. Sergeyev, Geochim. Cosmochim. Acta 60 (1996) 2495.
[61] G.S. Pokrovski, J. Schott, S. Salvi, R. Gout, J.D. Kubicki, Mineral. Mag. A 62 (1998) 1194.